Published in final edited form as:
Immunity. 2009 August 21; 31(2): 342–355. doi:10.1016/j.immuni.2009.06.023.

Dynamics of T cell, antigen presenting cell, and pathogen interactions during recall responses in the lymph node

Tatyana Chtanova,
Department of Molecular and Cell Biology, Life Sciences Addition, University of California, Berkeley, CA 94720 U.S.A

Seong-Ji Han,
Department of Molecular and Cell Biology, Life Sciences Addition, University of California, Berkeley, CA 94720 U.S.A

Marie Schaeffer,
Department of Molecular and Cell Biology, Life Sciences Addition, University of California, Berkeley, CA 94720 U.S.A

Giel G. van Dooren,
Center for Tropical & Emerging Global Diseases and Department of Cellular Biology, University of Georgia, Paul D. Coverdell Center 500 D.W. Brooks Drive, Athens, GA 30602

Paul Herzmark,
Department of Molecular and Cell Biology, Life Sciences Addition, University of California, Berkeley, CA 94720 U.S.A

Boris Striepen, and
Center for Tropical & Emerging Global Diseases and Department of Cellular Biology, University of Georgia, Paul D. Coverdell Center 500 D.W. Brooks Drive, Athens, GA 30602

Ellen A. Robey[2]
Department of Molecular and Cell Biology, Life Sciences Addition, University of California, Berkeley, CA 94720 U.S.A

Summary

Memory T cells circulate through lymph nodes where they are poised to respond rapidly upon re-exposure to a pathogen, however the dynamics of memory T cell, antigen presenting cell, and pathogen interactions during recall responses are largely unknown. We used a mouse model of infection with the intracellular protozoan parasite, *Toxoplasma gondii*, in conjunction with two-photon microscopy, to address this question. After challenge, memory T cells migrated more rapidly than naïve T cells, relocalized towards the subcapsular sinus (SCS) near invaded macrophages and engaged in prolonged interactions with infected cells. Parasite invasion of T cells occurred by direct transfer of the parasite from the target cell into the T cell, and corresponded to an antigen-specific increase in the rate of T cell invasion. Our results provide

[2]Corresponding Author: Ellen A. Robey, Ph.D., Department of Molecular and Cell Biology, 471 Life Sciences Addition, University of California, Berkeley, Berkeley, CA 94720; Phone: (510) 642-8669; Fax: (510) 643-9500; erobey@berkeley.edu.

insight into cellular interactions during recall responses and suggest a mechanism of pathogen subversion of the immune response.

Keywords

Two-photon; memory T cells; pathogen; *Toxoplasma gondii*

Introduction

Lymph nodes provide organized environments where primary and recall T cell responses are initiated. T cells and dendritic cells (DCs) are concentrated in the paracortical region of the lymph node, known as the T cell zone, and this region is an important site for T cell priming via DCs that have captured antigen in the periphery and then migrated into lymph nodes. However, recent studies have focused attention on the SCS as a site for the initiating adaptive immune responses (Carrasco and Batista, 2007; Hickman et al., 2008; Junt et al., 2007; Phan et al., 2007). In particular, a specialized subset of macrophages residing in the subcapsular sinus trap lymph-borne particulate antigens, and have been implicated in presenting antigen to B cells (Carrasco and Batista, 2007; Junt et al., 2007; Phan et al., 2007). In response to viral infection, T cells accumulate in the SCS and contact virus-containing cells (Hickman et al., 2008), however the APC populations for T cells in the SCS remain largely uncharacterized.

Like naive T cells, memory T cells are also concentrated in the T cell zone of the lymph node, where they are poised to rapidly initiate recall responses upon reencounter with a pathogen. Contact with antigen bearing cells in the lymph node can serve to increase the activation state of memory T cells and can trigger effector functions such as cytokine release and cell killing to control pathogen spread. The ability of memory T cells to migrate to sites of infection, and form contacts with infected cells could also be exploited by pathogens to target memory T cells for immune evasion mechanisms. Direct time-lapse visualization of T cells and antigen-presenting cells in intact lymph nodes by two-photon microscopy could provide insight into these events. While this approach has been extensively used to characterize T cell-DC interactions during priming in response to model antigens (reviewed in (Bousso, 2008; Cahalan and Parker, 2008)), it is just beginning to be applied to the study of antigen-experienced T cells (Boissonnas et al., 2007; Breart et al., 2008; Matheu et al., 2008; Mempel et al., 2006; Mrass et al., 2006) and in vivo response to infection (Egen et al., 2008; Hickman et al., 2008; Junt et al., 2007; Peters et al., 2008).

The intracellular protozoan parasite, *Toxoplasma gondii* provides an excellent experimental system for the study of T cell responses during infection. *T. gondii* is highly adapted to its mammalian hosts, and has evolved mechanisms to modulate host immunity to promote parasite spread and persistence while avoiding excessive mortality (Boothroyd and Dubremetz, 2008). During the acute phase of infection parasites disseminate widely through the body via lymphatics and circulation, but are eventually brought under control by a robust adaptive immune response (Denkers and Gazzinelli, 1998; Lieberman and Hunter, 2002; Yap and Sher, 1999). Parasites then persist as cysts in brain and muscle for the lifetime of the host, and CD8 T cells play a key protective role in both the acute and chronic phases of infection (Brown and McLeod, 1990; Gazzinelli et al., 1992; Gazzinelli et al., 1991; Suzuki and Remington, 1988). This is in spite of the fact that parasites reside in a specialized parasitophorous vacuole that limits access of parasite antigens to the host cytosol and the class I presentation pathway (reviewed in (Dzierszinski and Hunter, 2008; Plattner and Soldati-Favre, 2008)).

Here we used two-photon microscopy in conjunction with a mouse model of *T. gondii* infection to examine memory T cell responses in lymph nodes. We show that after challenge, memory T cells migrated more rapidly than naive T cells and relocalized to foci of infection at the SCS. Memory T cells engaged in prolonged interactions with both infected macrophages and DCs leading to the formation of antigen-specific stable T cell clusters at the SCS. Contacts with infected target cells exposed T cells to invasion, which occurred by simultaneous egress of parasites from the target cell and invasion of the T cell. T cells represented the major cell type containing parasites in the mesenteric lymph node and blood following oral infection, and blocking T cell egress after oral infection slowed parasite spread beyond the mesenteric lymph nodes. Our results shed light on the behavior of memory T cells during recall responses and suggest a potential mechanism whereby parasites may exploit the close contact of T cells to promote their own survival.

Results

Memory T cells co-localize with parasites at the subcapsular sinus

Upon exposure to live, attenuated *T. gondii* tachyzoites, mice develop lasting protective immunity to the parasite, with CD8 T cells playing a major protective role (Fox and Bzik, 2002; Gazzinelli et al., 1991). We have adapted this system to examine the dynamics of T cell, APC, and parasite interactions during recall responses. For these studies we engineered parasites to express a secreted version of the model antigen ovalbumin (OVA), a form that is recognized by CD8 T cells (Gubbels et al., 2005; Kwok et al., 2003). We also engineered the parasites to express a red fluorescent protein derivative (RFP) to allow for fluorescent imaging of the parasites. We then generated mice in which a subset of T cells were naive GFP-labeled OVA-specific CD8 T cells (OT1) T cells (Witt et al., 2005), immunized mice with irradiated parasites, and challenged >4 weeks later with live parasites. As expected, OT1 T cells showed antigen-dependent up-regulation of the activation marker CD69 three days after initial exposure to irradiated parasites expressing OVA (Fig. S1A), and one day following challenge (Fig. S1B). This corresponded with the ability of OT1 T cells to produce IFN-gamma after a brief in vitro-restimulation (Fig. S1). In addition, immunization with irradiated parasites protected animals from challenge with a lethal dose of live, non-irradiated parasites, protection that depended on the presence of CD8 T cells ((Gazzinelli et al., 1991; Suzuki and Remington, 1988) and data not shown). Memory CD8 T cells in this system were predominantly CD44+ but heterogeneous in terms of CD62L expression, suggesting they represented a mixture of effector and central memory cells (data not shown).

To obtain a rapid and synchronous recall response we challenged immunized mice using an earflap infection model. In this model parasites are found in the subcapsular sinus (SCS) of the draining lymph node hours after infection, within CD169+ macrophages and in the vicinity of neutrophil swarms (Chtanova et al., 2008). Fluorescent microscopy of frozen lymph node sections confirmed that at 5 hours after challenge many parasites were found inside CD169+ SCS macrophages, most of which co-stained with the parasite dense granule marker, GRA6, indicating that parasites resided within parasitophorous vacuoles (Fig. S2A). Analysis of lymph node sections from CD11cYFP reporter mice (Lindquist et al., 2004) confirmed that a subset of CD169+ macrophages expressed intermediate levels of the CD11cYFP reporter (Fig. S2B). This is in line with an earlier report showing that some SCS macrophages express low levels of CD11c (Junt et al., 2007). At 5 hours after challenge parasites were occasionally found associated with YFP high cells with DC-like morphology. By 24 hours after challenge many parasites were found in deeper regions of the lymph node associated with CD11c YFP high DCs (data not shown).

To examine how T cell localization in lymph nodes changed in response to challenge we used fluorescence microscopy to quantitate the density of memory T cells relative to the

capsule of the lymph node (Fig. 1A). We also injected mice with dye-labeled naïve OT1 T cells 24 hours prior to challenge to compare naïve and memory T cell behavior. In resting lymph nodes, naïve and memory T cells distributed throughout the T cell zone and were largely excluded from B cell follicles, with memory T cell density higher in more peripheral regions of the T cell zone and interfollicular areas compared to naïve T cells (Fig. 1A, B and C), consistent with reports of memory T cell localization in the spleen (Khanna et al., 2007). Five hours after challenge memory OT1 T cells became more concentrated in the subcapsular zone near foci of infection (Fig. 1A and B). We confirmed the change in T cell localization by plotting the distance from individual OT1 T cells to the lymph node capsule (Fig. 1C). The shorter average distance of memory T cells to the capsule and the higher proportion of memory T cells at the SCS compared to naive T cells were consistently seen in different quadrants of the same lymph nodes (Figure S3). Memory OT1 T cells localized closer to the infection sites even when the parasites did not express OVA (Fig. 1B and C). Taken together our results indicate that as early as 5 hours after challenge memory T cells undergo an antigen-independent redistribution towards the foci of infection in the SCS of the lymph node.

T cell recall response to T. gondii challenge visualized using two-photon microscopy

To examine the dynamic behavior of memory T cells in response to challenge we used two-photon microscopy of intact lymph nodes. To simultaneously image naive and memory antigen-specific T cells, immunized mice containing GFP-labeled memory OT1 T cells were adoptively transferred with fluorescent dye-labeled naïve OT1 T cells. In resting lymph nodes, memory T cells migrated at speeds similar to those of naïve T cells (Fig. 2A left panel, video 2Ai). However, 5 hours after challenge, memory T cells were significantly faster than naive T cells. This reflects both a slight increase in speed of memory T cells and a slight decrease in speed of naïve T cells relative to resting lymph nodes. The increase in speed of memory T cells occurred whether or not parasites expressed OVA (Fig. 2A, video 2Aii).

At one day after challenge the average speed of memory T cells decreased dramatically (Fig. 2A left panel). The drop in speed corresponded to a large proportion of T cells interacting with infected target cells (video 2Aiii) and coincided with increases in confinement ratio and arrest coefficient (Fig. S4). We also observed OT1 memory T cells engaging in cell division suggesting that at least some of the T cells have undergone antigen-specific TCR engagement (video 2Aiii).

To gain a better understanding of the early phase of the T cell recall response we focused on the 5 hour time point, by which time there was significant T cell redistribution toward foci of infection in the SCS (Fig. 1). While the majority of memory T cells migrated rapidly at this time point, a subset of T cells engaged in clusters of low motility indicative of antigen recognition (Fig. 2A middle panel and Fig. 2B, top panel, video 2B–C). The migration of two or more T cells in a confined region surrounding an exclusion zone of ~10 microns suggested that T cells were interacting with an unlabeled antigen presenting cell (Fig. 2B). The exclusion zone inside the T cell cluster usually contained one or more parasites (95 out of 109 clusters in 42 datasets, or 87%, Fig. 2A pie chart). Importantly, T cell clusters were not observed when mice were infected with parasites that did not express OVA (0 clusters in 13 datasets), indicating that T cell clustering is an antigen-dependent phenomenon. The majority of T cell clusters (97 out of 109 or 89%) persisted for the duration of the imaging runs (20–30 min, Fig. 2A pie chart). For those clusters that did break up during the imaging run, the rapid dispersal of T cells often corresponded to the sudden acquisition of parasite motility (Fig. 2B bottom panels, video 2B–C) consistent with target cell lysis and parasite egress (Moudy et al., 2001). This is consistent with the idea that contact with an intact infected cell is needed to maintain the T cell cluster.

We also noted examples of naïve and memory T cells participating in the same clusters (Fig. 2C, left panels, video 2B–C). To compare the ability of naive and memory T cells to participate in clusters, we recorded the number of T cells found in clusters relative to the number of each type of T cell found in the imaging volumes (Fig. 2C, right hand plot). By this measure, memory and naive T cells showed a similar ability to engage in contacts with infected cells. As with memory T cells, we never observed naive T cells dissociating from contacts, except in cases of target cell lysis (data not shown). Thus naive and memory T cells appear to have a similar ability to engage in long lasting contacts with infected cells.

To confirm that T cell clusters were the direct result of antigen presentation by infected cells, we challenged mice with equal mixtures of parasites that expressed OVA and control parasites that did not express OVA, and scored OT1 T cell clusters around infected cells (Fig. 2D and video 2D). We observed that OT1 T cell clusters formed around target cells with OVA only parasites, and around doubly infected (+ and – OVA parasites) cells, but very rarely around cells that contained only control (-OVA) parasites. The low frequency of clusters around control parasites is similar to the rate of clusters with no visible parasites (Fig. 2D), and was not increased even when the ratio of parasites was adjusted to increase the number of infected cells containing only -OVA parasites (data not shown). These results, together with the lack of OT1 T cell cluster formation when mice were challenged with parasites that did not express OVA, and the observation that most clusters from around parasite-containing cells, strongly imply that T cell clusters formed as a direct result of antigen recognition on an infected cell.

In addition, to these low motility T cell clusters, we also observed several parasite-memory T cell pairs moving coordinately, suggesting a tight contact between a motile unlabeled infected host cell and a T cell (Fig. S5, video S5). These motile conjugates were relatively infrequent (14 events observed out 94 runs, corresponding to 40 hours of cumulative imaging time). In all of the observed motile conjugates the infected cell led and the T cell followed, with the parasite (presumably inside an unlabeled infected cell) turning just before the T cell (Fig. S5 green and red arrows, video S5). Furthermore, the conjugate pairs moved at an average speed of 6 um/min, which was significantly lower than the speed of freely migrating T cells, and suggested that the infected cell determined the speed of the pair (Fig. 2A). These observations were reminiscent of T-B conjugates observed during helper T cell function, or CTL killing in intact lymph nodes (Mempel et al., 2006; Okada et al., 2005). Taken together these data suggest that as early as 5 hours after infection with *T. gondii* memory T cells can engage in long-lasting antigen-specific interaction with motile and non-motile infected cells.

T cells interact with DCs and SCS macrophages during recall response to T. gondii

In order to characterize the major cell types that serve as targets for memory T cells in the lymph node, we focused on the SCS macrophages, because they are positioned for initial contact with pathogens and are heavily infected after challenge with *Toxoplasma*, and on DCs, because of their potent ability to activate T cells. We initially used the CD11cYFP reporter that is expressed at high levels by DCs and at lower levels by a subset of CD169+ SCS macrophages (Fig S2B and (Junt et al., 2007)). Two-photon imaging of lymph nodes from reporter mice that had been immunized and then challenged with *Toxoplasma* revealed several examples of OT1 T cells engaged in lasting interactions with YFP high DCs (Fig. 3A, video 3A). Interestingly, the majority of T cell clusters surrounding DCs occurred with DCs that did not contain visible parasite fluorescence (Fig. 3A top and middle panels, video 3A). In addition to the CD11cYFP reporter high cells, we also detected a population of YFP low cells that lacked dendrites, and that tended to harbor larger numbers of parasites relative to the YFP high population, some of which correspond to SCS macrophages (Fig. S2, Fig. 3A bottom panel and bar graph). Of the T cell clusters scored in this analysis, 39% formed

around YFP low cells, 32% formed around YFP high cells, and 29% formed around APCs that did not express detectable levels of the CD11c YFP reporter, suggesting that together DCs and SCS macrophages constitute the major target populations in this setting.

Since the CD11cYFP reporter labels only a subset of CD169+ macrophages, we also labeled SCS macrophages by injecting fluorescently labeled CD169 antibody into the mouse earflap prior to imaging. CD169-labeled cells formed a continuous layer in the subcapsular area of the lymph node with memory T cells forming clusters within, and directly adjacent to, the layer of labeled macrophages (Figure 3B, Video 3Bi and Video 3Bii). For this analysis, we defined a T cell cluster as 2 or more OT1 T cells contacting a CD169+ cell for more than 10 minutes. Notably, most (38 out of 45 clusters or 84%) of the stable T cell contacts with SCS macrophages occurred with parasite-containing target cells (Fig. 3B). This is in contrast to the T cell clusters around DCs, of which only 30% surrounded DCs that contained visible parasites. Moreover, given the data from lymph node sections showing that the majority of infected CD169+ cells stained with the parasite dense granule protein, GRA6 (Fig. S2A) and that OT1 T cell contacts were observed only with CD169+ cells that contained GRA6 protein (Fig. S2A, hatched bar), these data indicated that T cells contacted actively infected SCS macrophages. Some contacts occurred as large clusters with more than 5 T cells surrounding an infected macrophage. We also noted several examples of T cell clusters that included both naïve and memory T cells surrounding a CD169 cell (Fig. 3B, video 3Bii). Our results demonstrate that T cells can form long-lasting interactions both with invaded SCS macrophages and DCs and indicate that SCS macrophages are a significant APC population for CD8 T cells at the early stages of infection.

Direct invasion of T cells by T. gondii during contacts with infected target cells

Recent evidence that parasite egress is linked to target cell killing by T cells (Persson et al., 2007) suggests that parasites could exploit the close contact between T cells and APC to facilitate cell to cell spread. To investigate whether this occurs in vivo we focused on the examples of T cell contacts with infected cells that dissociated during the imaging run. Parasites became highly motile upon target cell lysis (Fig. 2B and (Moudy et al., 2001) making it difficult to track the fate of individual parasites. However, in 3 out of 10 of observed instances of target cell lysis and T cell cluster break-up we found that the parasites invaded one of the T cells that had been in contact with the infected cell (Fig. 4A, video 4A). In addition to these examples in which T cell invasion was documented in the imaging run, we also noted many examples of T cells in imaging volumes that harbored parasites. In general T cells containing parasites remained motile and migrated with similar speeds to uninfected T cells (Fig. 4A). Confocal microscopy of lymph node tissue sections (Fig. 4B) and in vitro infected T cells (Fig. 4C) revealed that parasites inside T cells appeared intact, corresponded to a “hole” in fluorescence signal in T cells, and were surrounded by the parasite dense granule protein GRA6, consistent with the active invasion of T cells and the formation of a parasitophorous vacuole inside T cells.

Since the most common natural route of infection is through ingestion, we also examined T cells in the mesenteric lymph nodes after oral infection of naïve mice with *Toxoplasma* cysts. Following oral infection the parasites arrive asynchronously in the mesenteric lymph nodes and are found both in the subcapsular sinus and in deeper regions of the lymph node at 5–7 days after infection ((Chtanova et al., 2008) and data not shown). Two-photon microscopy of OT1 GFP T cells in the mesenteric lymph nodes of mice orally infected with OVA-expressing parasites revealed infected T cells migrating at comparable speeds to uninfected T cells in the same imaging volumes (Fig. 4D, left hand graph). We also observed examples of OT1 T cells being invaded by parasites while contacting infected target cells (Fig. 4D, right panels, video 4D–F).

To determine whether T cell invasion also occurred in the chronic phase of infection we examined the brains of infected mice. For these studies we infected mice with a low dose of a cyst-forming strain of RFP-OVA parasites and visualized T cell migration in vibratome-cut brain slices using two-photon microscopy (Schaeffer et al., 2009). Time-lapse imaging revealed invaded OT1 T cells actively migrating through the brain with average speeds and displacement rates within the range of those observed for OT1 T cells that did not contain parasites (Fig. 4E, video 4D–F). In addition we observed one instance of T cell invasion by *T. gondii* in the brain apparently while contacting an infected cell (Fig. 4F, video 4D–F). The detection of T cell invasion by parasites in 3 different infection settings indicates that T cell invasion by *T. gondii* is a general feature of infection with this intracellular parasite. Furthermore, invaded T cells remain motile suggesting a potential mechanism for parasite spread.

Enhancement of T cell invasion by antigen recognition

The observation that T cell invasion occurred while the T cell was making a tight contact with an infected cell suggested that contacts formed during antigen-specific interactions may have enhanced parasite egress and T cell invasion. If this were the case, we would expect to observe a higher rate of infection under conditions in which T cells can make antigen-dependent contacts with infected cells. To investigate this, we used flow cytometry to quantiate invaded T cells in draining lymph nodes following earflap injection. The infection of OVA-specific memory T cells in the presence of parasites expressing ovalbumin was substantially higher than for comparable rates of infection with parasites that did not express OVA, or for endogenous polyclonal CD8 T cells (Fig. 5A). This is consistent with the hypothesis that parasite invasion of T cells was enhanced by tight antigen-specific interactions between T cells and infected target cells. We also noted that, although both naive and memory OT1 T cells showed a higher rate of infection compared to polyclonal T cells, memory T cells had a consistently higher rate of infection when compared to naive OT1 T cells in the same lymph nodes (Fig. 5B). This is consistent with our observation that both memory and naive OT1 T cells form tight contacts with infected cells, but that memory T cells showed a more extensive relocalization to the SCS upon challenge (Fig. 1B, C).

T cells accounted for half of all the infected leukocytes in the mesenteric lymph nodes at day 7 after oral infection (Fig. 5C, pie graph). Moreover, a high proportion of T cells containing parasites expressed the activation marker CD69, suggesting that the invaded T cells had recently encountered antigen (Fig. 5C, right hand plot). Although DCs and macrophages were more infected on a proportional basis (2% of DC and macrophages infected and 0.7% of T cells) they made up a smaller proportion of all infected cells due to their lower numbers in mesenteric lymph nodes (data not shown). Infected endogenous T cells (CD3+) could also be detected in circulation 7 days after oral infection, and represented approximately half of all infected cells detected in the blood (Fig. 5D).

To more directly examine the impact of antigen-recognition on T cell invasion, we compared OT1 T cells to T cells expressing an irrelevant TCR (P14 TCR, (Pircher et al., 1989)). Seven days after oral infection, OT1 T cells expanded to make up ~50% of CD8 T cells in the mesenteric lymph node (Fig. S6A). In contrast P14 T cells generally represented less than 4% of CD8 T cells, in spite of the fact that P14 and OT1 T cells were present at a 5:1 ratio in the initial transfer. Similar T cell numbers were seen in spleen (Fig. S6A) and non-draining lymph nodes (data not shown). There was also a 3–5x increase in the rate of infection of OT1 T cells compared to P14 T cells in mesenteric lymph nodes and spleen (Fig. S6B). This increase in the rate of infection, together with the greater expansion of OT1 T cells, led to an approximately 100-fold increase in the number of infected OT1 T cells versus infected P14 T cells in the mesenteric lymph nodes (Fig. S6C). Together these data imply that antigen-specific T cells are a major population that harbors parasites during

Toxoplasma infection, due both to their expansion and recruitment to sites of infection, and because of their direct contact with infected target cells.

Blocking T cell egress from lymph nodes inhibited parasite spread

The high rate of infected T cells in mesenteric lymph node and blood following oral infection, together with the observation that invaded T cells remained motile, suggested that parasites could exploit T cells to promote their dissemination within the infected host. Consistent with this model, injection of FACS-sorted invaded T cells into naive mice resulted in active infection in draining lymph nodes and spleens 5 days later (Fig. 6A), indicating that parasites within T cells remained viable and infectious. In addition, invaded T cells could be detected in lymph nodes 2–4 hours after i.v. injection of infected T cells (data not shown), implying that invaded T cells retained the ability to traffic in the body. Finally, we asked whether blocking T cell egress from lymph nodes could inhibit parasite spread. For this experiments, we used the oral route of infection, in which parasites and antigen specific T cells were first detectable in gut-draining mesenteric lymph nodes before accumulating in other parts of the body during the first week of infection (Fig. 6, Fig. S6 and (Courret et al., 2006)). After oral infection, we treated mice every other day with FTY720, a drug that acts on the S1P1 receptor to block T cell egress from the lymph node, and examined parasite number 7 days post infection (Fig. 6B). We found that FTY720 treatment significantly reduced the number of parasites detected in spleen and non-draining lymph nodes, but did not affect the numbers in the mesenteric lymph nodes, suggesting that sequestering infected T cells in the mesenteric lymph nodes prevented parasite spread. Together these data support the view that invaded T cells help to spread infection by transporting viable parasites from lymph nodes to other parts of the body.

Discussion

We have used a *Toxoplasma gondii*- mouse infection model, in conjunction with two-photon microscopy to visualize memory CD8 T cells, APCs, and parasites in intact lymph nodes. Memory T cells formed stable antigen-specific clusters near invaded macrophages at the SCS, and made stable contacts with both actively invaded SCS macrophages, and DCs, some of which did not contain visible parasites. While naive T cells also formed stable contacts with infected cells, memory T cells showed more rapid migration and more extensive relocalization toward foci of infection in the subcapsular region of the lymph node. Tight contacts with infected cells exposed T cells_to invasion by parasites, which occurred by direct relocation of the parasite from the target cell to the T cell. Invaded T cells remained motile and constituted a large proportion of parasitized cells in the mesenteric lymph node and in circulation 7 days after oral infection. Our study characterizes the dynamics of memory T cell interactions with infected cells in lymph nodes and uncovers a potential mechanism whereby parasites may exploit the close contact between T cells and infected antigen presenting cells to promote their own survival.

Particulate antigens and pathogens arriving via the lymphatics are retained in the subcapsular region of the lymph node (Abadie et al., 2005; Carrasco and Batista, 2007; Chtanova et al., 2008; Junt et al., 2007; Phan et al., 2007) and naive T cells can relocalize to the subcapsular region in response to viral infection (Hickman et al., 2008). Here we show that, in response to ear-flap challenge with *T. gondii*, both memory and naive T cells reposition from the T cell zone to the foci of infection in the subcapsular region of the draining lymph node. In contrast to the mostly antigen-dependent relocalization seen upon viral infection (Hickman et al., 2008), T cell relocalization to the subcapsular region during *T. gondii* infection was antigen-independent, suggesting a response to chemoattractants produced locally at foci of infection. Preliminary RNA analysis indicated that multiple chemokines were induced in lymph nodes following Toxoplasma challenge (data not

shown), consistent with reports of induction of chemokines by Toxoplasma in other systems (reviewed in (Denkers et al., 2004; Kasper et al., 2004)). SCS macrophages that harbor many parasites, neutrophils that are recruited to draining lymph nodes at early times after infection (Chtanova et al., 2008), and non-hematopoetic cells are all potential sources for these chemoattractants.

A key function of immunological memory is to provide a faster and stronger response upon re-encounter with the same antigen. We found that memory T cells migrated significantly faster than naïve T cells after challenge and showed a more extensive relocalization towards the foci of infection, as indicated both by their location relative to parasites in lymph node tissue sections (Fig. 1B,C), and the higher rate of infection of memory T cells relative to naive T cells of the same specificity within the same lymph nodes (Fig. 5B). Thus while both memory and naive T cells are capable of engaging in lasting contacts with parasite infected cells, memory T cells have a greater ability than naive T cells to migrate toward sites of infection. This difference, together with other factors such as higher frequency of antigen specificity and greater sensitivity to TCR triggering (Sprent and Surh, 2001), may contribute to the shorter response

SCS macrophages can present antigen to B cells (Carrasco and Batista, 2007; Junt et al., 2007; Phan et al., 2007), in line with their ability to trap and retain antigen on their surface, rather than internalize and degrade it (Fossum, 1980; Szakal et al., 1983). The observation that *T. gondii* parasites were found inside SCS macrophages surrounded by the parasite dense granule protein GRA6, implies that Toxoplasma actively invaded the macrophages, and established themselves in parasitophorous vacuoles, compartments that do not fuse with endosomes and provide a protective, environment for parasite replication (Joiner et al., 1990). Together these observations suggest that when an intracellular pathogen such as Toxoplasma arrives at the SCS it may be initially trapped by, and then invade the macrophage, whereupon its antigens may become visible to CD8 T cells.. SCS macrophages may be less likely to serve as antigen presenting cells for CD4 T cells that focus on endocytosed antigens. The function of SCS macrophages as APCs for memory CD8 T cells may also be restricted to the early phase of recall responses, when the pathogens first arrive in the SCS. Indeed, we observe that at later time points, parasites gain access to deeper regions of the lymph node, which may result from the removal of SCS macrophages by neutrophils (Chtanova et al., 2008), and/or the lysis of infected macrophages by parasite egress and T cell killing.

In addition to SCS macrophages, we also observed T cells forming clusters around DCs near the lymph node capsule. Unlike SCS macrophages, the majority of DC that attracted the notice of T cells did not contain visible parasite fluorescence. This could be a reflection of the ability of DC to cross-present parasite antigens. However, given previous indications that Toxoplasma antigens are presented via the classic MHC-1 pathway by actively invaded APCs (Dzierszinski et al., 2007; Goldszmid et al., 2009; Gubbels et al., 2005)), together with evidence that some host cells can destroy parasites within parasitophorous vacuoles (Andrade et al., 2006; Zhao et al., 2009), we favor the view that parasites initially invaded DC but were then destroyed, leading to the loss of parasite fluorescence but the retention of antigen-MHC complexes on the DC surface.

One unexpected aspect to this study was the observation of parasites moving directly from an infected target cell into a T cell during antigen-dependent contacts. We observed multiple examples of such events in different infection settings including draining lymph nodes following earflap challenge, mesenteric lymph nodes after oral infection, and brain during chronic infection. These examples, together with the high proportion of parasitized T cells in mesenteric lymph nodes and blood following oral infection, and the antigen-dependent

increase in T cell invasion, implies that invasion of T cells during antigen-dependent contacts is a prominent feature of *Toxoplasma* infection in vivo.

A number of factors may contribute to the high rate of infection of T cells. One factor is the tight cell-to cell contact with an infected cell that occurs during antigen recognition. Intimate contacts between T cells and infected cells were frequently observed, and preceded all of the invasion events that we observed. Second, based on recent reports that Fas-FasL interactions and perforin release can trigger parasite egress (Persson et al., 2007), and given that the lasting CD8 T cell-target cell contacts that we observed may have resulted in target cell killing, it seems likely that release of cytotoxic granules by the T cell could also promote antigen-specific invasion of the T cell by parasites. Thus an immunological synapse formed between T cell and infected cell could help to guide and couple parasite egress and invasion, whereas target cell killing by cytotoxic T cells could help to trigger these events. Transfer of parasites via an organized cell-cell contact region would be analogous to the virological synapses that have been implicated in cell-to-cell spread by viruses, such as HIV (Piguet and Sattentau, 2004). Finally, our data indicates that antigen-specific T cells are preferentially expanded and recruited to mesenteric lymph nodes after oral infection, and that this contributes to their preferential infection in vivo.

Invasion of T cells could provide a means for parasites to disseminate throughout the body. While *T. gondii* tachyzoites are highly motile outside of host cells, transport inside a T cell could allow access to a variety of tissues, and would also protect the parasite from components of the humoral immune system. While earlier reports have suggested that DCs and macrophages can be hijacked by the parasites for dissemination (Courret et al., 2006; Lambert et al., 2006), the data presented here showing that invaded T cells comprise the major population of infected cells in the blood and lymph node after oral infection, implies that T cells may also contribute to parasite spread. Moreover, the observation that FTY720 treatment, which led to a drop in T cells, but not DCs in blood (data not shown), led to a reduction in parasite load in the periphery following oral infection, also supports a role for T cells in parasite dissemination.

Invasion of antigen-specific T cells may also provide an opportunity for the parasite to modulate the immune response from the ‘inside’ by controlling the survival and functionality of the *Toxoplasma-specific* T cells. During invasion *T. gondii* secretes a number of proteins into the host cytosol. At least some of these proteins, such as ROP16, are able to interact with the host cell machinery to modify the host cell function including the production of immune response mediators (reviewed in (Boothroyd and Dubremetz, 2008)). The targeting of antigen-specific T cells highlights the delicate interplay between the host’s immune system and a successful pathogen such as *T. gondii.* While CD8 T cells are crucial for protection of the host, *Toxoplasma* may have evolved ways to target and exploit these cells for their own advantage.

Experimental Procedures

Mice

All mice were bred and housed in pathogen-free conditions at the AALAC-approved animal facility at Life Science Addition, University of California, Berkeley. All animal experiments were approved by the Animal Care and Use Committee of UC Berkeley. Ubiquitin-GFP mice (Schaefer et al., 2001) were a gift from Brian Schaefer. CD11cYFP transgenic reporter mice (Lindquist et al., 2004) and actin promoter CFP transgenic mice (Hadjantonakis et al., 2002) were provided by Michel Nussenzweig’s laboratory. Bone marrow donors were UBI-GFP or actin-CFP transgenic mice crossed to OT1 TCR transgenic mice Rag2-/- mice (purchased from Taconic) to generate GFP or CFP OT1 TCR transgenic Rag2-/- donors. In

order to generate mice with a small number of OT1 T cells we injected bone marrow from OT1 Rag2- GFP mice into newborn C57BL/6 or CD11cYFP mice as described (Witt et al., 2005). In some experiments naïve T cells either from P14 TCR transgenic mice ((Pircher et al., 1989)) purchased from Taconic), OT1 Rag2- CFP mice or from OT1 Rag2-/- mice labelled with SNARF or CellTracker Orange according to manufactures instructions (Invitrogen) (2×10^7 /mouse) were transferred by tail vein injection 24 hours prior to infection and/or imaging.

Parasites

Generation of *T. gondii* cell lines expressing the tandem (td) Tomato variant of red fluorescent protein (RFP) (Shaner et al., 2004) and ovalbumin were described previously (Chtanova et al, 2008)(Schaeffer et al 2009). All parasites were maintained in confluent human foreskin fibroblasts.

For mouse infections, parasites were prepared from almost lysed fibroblast cultures by first releasing the parasites from fibroblasts by passing them through 21g 1½ gauge and 23g1 needles 5–10 times. Parasites were then filtered through a 3 μm filter, pelleted and resuspended in phosphate-buffered saline. 5×10^6–1×10^7 parasites (typically 5×10^6) in 10 μl volume were injected into the earflap. For immunizations, mice were injected with 10^6 irradiated parasites intraperitoneally at least 4 weeks prior to infection and imaging.

For oral infections, cysts were isolated from brain homogenates of CBA/J mice (Jackson Laboratory, Bar Harbor, Maine) infected with 300–400 parasites i.p. 4–6 months prior. Cysts were counted after staining with Dolichos Biflorus Agglutinin (Vector Laboratories, Burlingame, CA). Mice were infected with 50–75 cysts by gavage. Mesenteric lymph nodes were used for microscopy or analyzed by flow cytometry. In experiment to test the role of T cell egress, FTY720 was administered every other day intravenously starting one day after oral infection with 75 cysts at the dose of 1 mg/kg. Mice were sacrificed and analyzed on day 7 after infection.

Antibodies and flow cytometry

Lymph nodes were dissociated by collagenase digestion. Cell suspensions were filtered, stained and analyzed by flow cytometry. The following antibodies were from eBioscience: phycoerythrin-Cy5 conjugated anti-CD11b (clone M1/70), and phycoerythrin-Cy5 conjugated anti-CD11c (clone N418). Fluorescein isothiocyanate-conjugated anti-CD169 antibody (clone 3D6.112) was purchased from AbD Serotec. Acquisitions were performed with a Coulter Epics XL-MCL flow cytometer (Beckman-Coulter) and data were analyzed with the FlowJo software (Tree Star, Ashland, Oreg.)._GRA6 staining to visualize the parasitophorous vacuole was performed using the anti-GRA6 rabbit antiserum obtained from Dr D. Sibley (Labruyere et al., 1999).

Statistical analysis

Values were expressed as mean ± standard error (SE). Levels of significance were calculated by unpaired *t* tests using the GraphPad Prism program (San Diego, CA, US). Differences were considered significant at $P<0.05$.

Two-photon Imaging

Mice were sacrificed at indicated times post infection, and dorsal cervical (draining lymph nodes for ear-flap infections) or mesenteric (for oral infections) lymph nodes were isolated and imaged by Two-Photon Laser Scanning Microscopy (TPLSM) while being perfused with warmed, oxygenated medium as described previously (Witt et al., 2005). For imaging T cell interactions with CD169 cells, 10–20 ul of neat in-house labeled CD169 antibody was

injected into the mouse ear-flap 5 minutes prior to sacrifice. For two-color microscopy, imaging volumes (164 × 164 × 40 microns) were scanned every 37 seconds for 20–40 minutes using an upright Zeiss 510 META/NLO 2p Microscope with Spectra-Physics MaiTai Laser. Two-photon excitation was achieved using a Spectra-Physics MaiTai laser tuned to 920nm, and GFP and YFP emission light was separated using a 515nm dichroic mirror and collected using two non-descanned detectors.

For three- and four-color microscopy, imaging volumes of 172 × 143 × 80 micron were generated using a custom-built microscope with a Spectra-Physics MaiTai Laser tuned to 900–920 nm. The emission light was separated using 495, 515 and 560 dichroics and collected using 4 detectors. Bandpass filters HQ 450/80M and HQ 645/75M were used to minimize spectral overlap.

Typical imaging volumes (164 × 164 × 40 microns or 172×143×80 microns respectively) corresponded to regions of the lymph nodes extending up to 200 microns below the surface of the capsule and were scanned every 13–37 seconds for 20–40 minutes. Mesenteric lymph nodes were imaged under similar conditions 5–7 days after oral infection. Chronic infection and imaging of T cells in the brain were performed as described previously (Schaeffer et al, 2009).

Data Analysis

The x,y,z co-ordinates of individual cells over time were obtained using Imaris Bitplane Software. Motility parameters were calculated using Matlab (Mathworks Inc., Boston; code available upon request). Parameters reported here include average peed (defined as path length over time; microns/minute), instantaneous speed (pathlength between 2 time points, averaged over successive 3 time points), arrest coefficient (percentage of time points when instantaneous speed is below 2 um/min), confinement ratio (ratio of maximum displacement to pathlength). GraphPad Prism was used for graphing and statistical analysis. Video were processed and recorded using Imaris Bitplane and ImageJ software. Gaussian filter was applied to reduce background noise.

Immunofluorescence microscopy

Isolated lymph nodes were fixed with 4% formalin/10% sucrose in PBS for 1 hr, sequentially submerged in 10, 20, 30 % sucrose for 18–24 hrs each, and frozen over dry ice in OCT. Serial 20 micron sections were generated by cryosectioning (MICROM H550,Microm GmbH, Walldorf, Germany) and stored at −80°C. Sections were brought to room temperature, fixed with cold acetone for 10 min, air dried and incubated with 10% mouse serum in Fc blocking reagent (2.4G2 culture supernatant) for 1hr. The tissue was stained with unconjugated anti-Ly6G (BD Biosciences), purified rat anti mouse CD169 (AbD Serotec), or biotin-conjugated anti-LYVE-1 (R&D systems) overnight at 4°C. After primary staining slides were washed 4x in PBS and incubated with either anti-rat Alexa 647 or streptavidin Alexa 633 (Invitrogen) for 2 hrs at room temperature. For GRA6 staining, slides were fixed with 3% PFA at room temperature for 20 min, washed twice in PBS and incubated for 15 min with PBS/0.1M glycine at room temperature. Staining with anti-GRA6 rabbit serum was performed in PBS/0.2% BSA/0.05% Saponin for 1 hour at room temperature. The slides were then washed and stained with an anti-rabbit secondary antibody for 20 min using the same buffer as for primary staining. After staining, sections were washed 4x in PBS and coverslipped using VectaShield (Vector Laboratories, Burlingame, CA) mounting medium, and visualized on Zeiss 510 Axioplan META NLO upright confocal microscope with a 10x air objective (Plan-Neofluar 10x/0,3) and a 40x oil objective (Plan-Neofluar 40x/1.3 oil WD=0.17mm) using 488nm, 543nm and 633nm laser lines. Images were analyzed and assembled using Adobe Photoshop and Imaris Bitplane.

Cell density was calculated using Matlab (Mathworks Inc., Boston; code available upon request).

Supplementary Material

Refer to Web version on PubMed Central for supplementary material.

Acknowledgments

The authors would like to thank Dr. Ena Ladi for help with motility calculations, Dr Zeev Bomzon for help with density calculations, Kumar Garapaty for help with Matlab, Shiao Chan for technical assistance, Holly Aaron for help with confocal microscopy. Hector Nolla and Alma Valeros, UC Berkeley CRL flow cytometry facility and Julie Nelson, CTEGD Flow Cytometry Facility for help with flow cytometry, N. Blanchard, P. Bousso, and members of the Robey lab for useful suggestions and proofreading of the manuscript. This work was funded by the NIH (BS and ER), Human Frontier Science Program Fellowship (TC), and C.J. Martin Overseas Fellowship (400489) from the Australian National Health and Medical Research Council (GvD).

Abbreviations

APC	antigen presenting cell
GFP	green fluorescent protein
YFP	yellow fluorescent protein
CFP	cyan fluorescent protein
RFP	red fluorescent protein
DC	dendritic cell
OVA	ovalbumin antigen
SCS	subcapsular sinus.

References

Abadie V, Badell E, Douillard P, Ensergueix D, Leenen PJ, Tanguy M, Fiette L, Saeland S, Gicquel B, Winter N. Neutrophils rapidly migrate via lymphatics after Mycobacterium bovis BCG intradermal vaccination and shuttle live bacilli to the draining lymph nodes. Blood. 2005; 106:1843–1850. [PubMed: 15886329]

Andrade RM, Wessendarp M, Gubbels MJ, Striepen B, Subauste CS. CD40 induces macrophage anti-Toxoplasma gondii activity by triggering autophagy-dependent fusion of pathogen-containing vacuoles and lysosomes. J Clin Invest. 2006; 116:2366–2377. [PubMed: 16955139]

Barragan A, Sibley LD. Transepithelial migration of Toxoplasma gondii is linked to parasite motility and virulence. J Exp Med. 2002; 195:1625–1633. [PubMed: 12070289]

Boissonnas A, Fetler L, Zeelenberg IS, Hugues S, Amigorena S. In vivo imaging of cytotoxic T cell infiltration and elimination of a solid tumor. J Exp Med. 2007; 204:345–356. [PubMed: 17261634]

Boothroyd JC, Dubremetz JF. Kiss and spit: the dual roles of Toxoplasma rhoptries. Nat Rev Microbiol. 2008; 6:79–88. [PubMed: 18059289]

Bousso P. T-cell activation by dendritic cells in the lymph node: lessons from the movies. Nat Rev Immunol. 2008

Breart B, Lemaitre F, Celli S, Bousso P. Two-photon imaging of intratumoral CD8+ T cell cytotoxic activity during adoptive T cell therapy in mice. J Clin Invest. 2008; 118:1390–1397. [PubMed: 18357341]

Brown CR, McLeod R. Class I MHC genes and CD8+ T cells determine cyst number in Toxoplasma gondii infection. J Immunol. 1990; 145:3438–3441. [PubMed: 2121825]

Cahalan MD, Parker I. Choreography of cell motility and interaction dynamics imaged by two-photon microscopy in lymphoid organs. Annu Rev Immunol. 2008; 26:585–626. [PubMed: 18173372]

Carrasco YR, Batista FD. B cells acquire particulate antigen in a macrophage-rich area at the boundary between the follicle and the subcapsular sinus of the lymph node. Immunity. 2007; 27:160–171. [PubMed: 17658276]

Chtanova T, Schaeffer M, Han SJ, van Dooren GG, Nollmann M, Herzmark P, Chan SW, Satija H, Camfield K, Aaron H, et al. Dynamics of neutrophil migration in lymph nodes during infection. Immunity. 2008; 29:487–496. [PubMed: 18718768]

Courret N, Darche S, Sonigo P, Milon G, Buzoni-Gatel D, Tardieux I. CD11c- and CD11b–expressing mouse leukocytes transport single Toxoplasma gondii tachyzoites to the brain. Blood. 2006; 107:309–316. [PubMed: 16051744]

Denkers EY, Butcher BA, Del Rio L, Bennouna S. Neutrophils, dendritic cells and Toxoplasma. Int J Parasitol. 2004; 34:411–421. [PubMed: 15003500]

Denkers EY, Gazzinelli RT. Regulation and function of T-cell-mediated immunity during Toxoplasma gondii infection. Clin Microbiol Rev. 1998; 11:569–588. [PubMed: 9767056]

Dzierszinski F, Pepper M, Stumhofer JS, LaRosa DF, Wilson EH, Turka LA, Halonen SK, Hunter CA, Roos DS. Presentation of Toxoplasma gondii antigens via the endogenous major histocompatibility complex class I pathway in nonprofessional and professional antigen-presenting cells. Infect Immun. 2007; 75:5200–5209. [PubMed: 17846116]

Dzierszinski FS, Hunter CA. Advances in the use of genetically engineered parasites to study immunity to Toxoplasma gondii. Parasite Immunol. 2008; 30:235–244. [PubMed: 18194347]

Egen JG, Rothfuchs AG, Feng CG, Winter N, Sher A, Germain RN. Macrophage and T cell dynamics during the development and disintegration of mycobacterial granulomas. Immunity. 2008; 28:271–284. [PubMed: 18261937]

Fossum S. The architecture of rat lymph nodes. IV. Distribution of ferritin and colloidal carbon in the draining lymph nodes after foot-pad injection. Scand J Immunol. 1980; 12:433–441. [PubMed: 7466330]

Fox BA, Bzik DJ. De novo pyrimidine biosynthesis is required for virulence of Toxoplasma gondii. Nature. 2002; 415:926–929. [PubMed: 11859373]

Gazzinelli R, Xu Y, Hieny S, Cheever A, Sher A. Simultaneous depletion of CD4+ and CD8+ T lymphocytes is required to reactivate chronic infection with Toxoplasma gondii. J Immunol. 1992; 149:175–180. [PubMed: 1351500]

Gazzinelli RT, Hakim FT, Hieny S, Shearer GM, Sher A. Synergistic role of CD4+ and CD8+ T lymphocytes in IFN-gamma production and protective immunity induced by an attenuated Toxoplasma gondii vaccine. J Immunol. 1991; 146:286–292. [PubMed: 1670604]

Goldszmid RS, Coppens I, Lev A, Caspar P, Mellman I, Sher A. Host ER-parasitophorous vacuole interaction provides a route of entry for antigen cross-presentation in Toxoplasma gondii-infected dendritic cells. J Exp Med. 2009

Gubbels MJ, Striepen B, Shastri N, Turkoz M, Robey EA. Class I major histocompatibility complex presentation of antigens that escape from the parasitophorous vacuole of Toxoplasma gondii. Infect Immun. 2005; 73:703–711. [PubMed: 15664908]

Hadjantonakis AK, Macmaster S, Nagy A. Embryonic stem cells and mice expressing different GFP variants for multiple non-invasive reporter usage within a single animal. BMC Biotechnol. 2002; 2:11. [PubMed: 12079497]

Hickman HD, Takeda K, Skon CN, Murray FR, Hensley SE, Loomis J, Barber GN, Bennink JR, Yewdell JW. Direct priming of antiviral CD8+ T cells in the peripheral interfollicular region of lymph nodes. Nat Immunol. 2008; 9:155–165. [PubMed: 18193049]

Joiner KA, Fuhrman SA, Miettinen HM, Kasper LH, Mellman I. Toxoplasma gondii: fusion competence of parasitophorous vacuoles in Fc receptor-transfected fibroblasts. Science. 1990; 249:641–646. [PubMed: 2200126]

Junt T, Moseman EA, Iannacone M, Massberg S, Lang PA, Boes M, Fink K, Henrickson SE, Shayakhmetov DM, Di Paolo NC, et al. Subcapsular sinus macrophages in lymph nodes clear lymph-borne viruses and present them to antiviral B cells. Nature. 2007; 450:110–114. [PubMed: 17934446]

Kasper L, Courret N, Darche S, Luangsay S, Mennechet F, Minns L, Rachinel N, Ronet C, Buzoni-Gatel D. Toxoplasma gondii and mucosal immunity. Int J Parasitol. 2004; 34:401–409. [PubMed: 15003499]

Khanna KM, McNamara JT, Lefrancois L. In situ imaging of the endogenous CD8 T cell response to infection. Science. 2007; 318:116–120. [PubMed: 17916739]

Kwok LY, Lutjen S, Soltek S, Soldati D, Busch D, Deckert M, Schluter D. The induction and kinetics of antigen-specific CD8 T cells are defined by the stage specificity and compartmentalization of the antigen in murine toxoplasmosis. J Immunol. 2003; 170:1949–1957. [PubMed: 12574363]

Labruyere E, Lingnau M, Mercier C, Sibley LD. Differential membrane targeting of the secretory proteins GRA4 and GRA6 within the parasitophorous vacuole formed by Toxoplasma gondii. Mol Biochem Parasitol. 1999; 102:311–324. [PubMed: 10498186]

Lambert H, Hitziger N, Dellacasa I, Svensson M, Barragan A. Induction of dendritic cell migration upon Toxoplasma gondii infection potentiates parasite dissemination. Cell Microbiol. 2006; 8:1611–1623. [PubMed: 16984416]

Lieberman LA, Hunter CA. The role of cytokines and their signaling pathways in the regulation of immunity to Toxoplasma gondii. Int Rev Immunol. 2002; 21:373–403. [PubMed: 12486820]

Lindquist RL, Shakhar G, Dudziak D, Wardemann H, Eisenreich T, Dustin ML, Nussenzweig MC. Visualizing dendritic cell networks in vivo. Nat Immunol. 2004; 5:1243–1250. [PubMed: 15543150]

Matheu MP, Beeton C, Garcia A, Chi V, Rangaraju S, Safrina O, Monaghan K, Uemura MI, Li D, Pal S, et al. Imaging of effector memory T cells during a delayed-type hypersensitivity reaction and suppression by Kv1.3 channel block. Immunity. 2008; 29:602–614. [PubMed: 18835197]

Mempel TR, Pittet MJ, Khazaie K, Weninger W, Weissleder R, von Boehmer H, von Andrian UH. Regulatory T cells reversibly suppress cytotoxic T cell function independent of effector differentiation. Immunity. 2006; 25:129–141. [PubMed: 16860762]

Moudy R, Manning TJ, Beckers CJ. The loss of cytoplasmic potassium upon host cell breakdown triggers egress of Toxoplasma gondii. J Biol Chem. 2001; 276:41492–41501. [PubMed: 11526113]

Mrass P, Takano H, Ng LG, Daxini S, Lasaro MO, Iparraguirre A, Cavanagh LL, von Andrian UH, Ertl HC, Haydon PG, Weninger W. Random migration precedes stable target cell interactions of tumor-infiltrating T cells. J Exp Med. 2006; 203:2749–2761. [PubMed: 17116735]

Okada T, Miller MJ, Parker I, Krummel MF, Neighbors M, Hartley SB, O'Garra A, Cahalan MD, Cyster JG. Antigen-engaged B cells undergo chemotaxis toward the T zone and form motile conjugates with helper T cells. PLoS Biol. 2005; 3:e150. [PubMed: 15857154]

Persson EK, Agnarson AM, Lambert H, Hitziger N, Yagita H, Chambers BJ, Barragan A, Grandien A. Death receptor ligation or exposure to perforin trigger rapid egress of the intracellular parasite Toxoplasma gondii. J Immunol. 2007; 179:8357–8365. [PubMed: 18056381]

Peters NC, Egen JG, Secundino N, Debrabant A, Kimblin N, Kamhawi S, Lawyer P, Fay MP, Germain RN, Sacks D. In vivo imaging reveals an essential role for neutrophils in leishmaniasis transmitted by sand flies. Science. 2008; 321:970–974. [PubMed: 18703742]

Phan TG, Grigorova I, Okada T, Cyster JG. Subcapsular encounter and complement-dependent transport of immune complexes by lymph node B cells. Nat Immunol. 2007; 8:992–1000. [PubMed: 17660822]

Piguet V, Sattentau Q. Dangerous liaisons at the virological synapse. J Clin Invest. 2004; 114:605–610. [PubMed: 15343375]

Pircher H, Burki K, Lang R, Hengartner H, Zinkernagel RM. Tolerance induction in double specific T-cell receptor transgenic mice varies with antigen. Nature. 1989; 342:559–561. [PubMed: 2573841]

Plattner F, Soldati-Favre D. Hijacking of host cellular functions by the Apicomplexa. Annu Rev Microbiol. 2008; 62:471–487. [PubMed: 18785844]

Schaefer BC, Schaefer ML, Kappler JW, Marrack P, Kedl RM. Observation of antigen-dependent CD8+ T-cell/ dendritic cell interactions in vivo. Cell Immunol. 2001; 214:110–122. [PubMed: 12088410]

Schaeffer M, Han SJ, Chtanova T, van Dooren GG, Herzmark P, Striepen B, Robey EA. Dynamic imaging of T cell - parasite interactions in the brains of mice chronically infected with Toxoplasma gondii. Journal of Immunology. 2009 in press.

Shaner NC, Campbell RE, Steinbach PA, Giepmans BN, Palmer AE, Tsien RY. Improved monomeric red, orange and yellow fluorescent proteins derived from Discosoma sp. red fluorescent protein. Nat Biotechnol. 2004; 22:1567–1572. [PubMed: 15558047]

Sprent J, Surh CD. Generation and maintenance of memory T cells. Curr Opin Immunol. 2001; 13:248–254. [PubMed: 11228420]

Suzuki Y, Remington JS. Dual regulation of resistance against Toxoplasma gondii infection by Lyt-2+ and Lyt-1+, L3T4+ T cells in mice. J Immunol. 1988; 140:3943–3946. [PubMed: 3259601]

Szakal AK, Holmes KL, Tew JG. Transport of immune complexes from the subcapsular sinus to lymph node follicles on the surface of nonphagocytic cells, including cells with dendritic morphology. J Immunol. 1983; 131:1714–1727. [PubMed: 6619542]

Witt CM, Raychaudhuri S, Schaefer B, Chakraborty AK, Robey EA. Directed migration of positively selected thymocytes visualized in real time. PLoS Biol. 2005; 3:e160. [PubMed: 15869324]

Yap GS, Sher A. Cell-mediated immunity to Toxoplasma gondii: initiation, regulation and effector function. Immunobiology. 1999; 201:240–247. [PubMed: 10631573]

Zhao YO, Khaminets A, Hunn JP, Howard JC. Disruption of the Toxoplasma gondii parasitophorous vacuole by IFNgamma-inducible immunity-related GTPases (IRG proteins) triggers necrotic cell death. PLoS Pathog. 2009; 5:e1000288. [PubMed: 19197351]

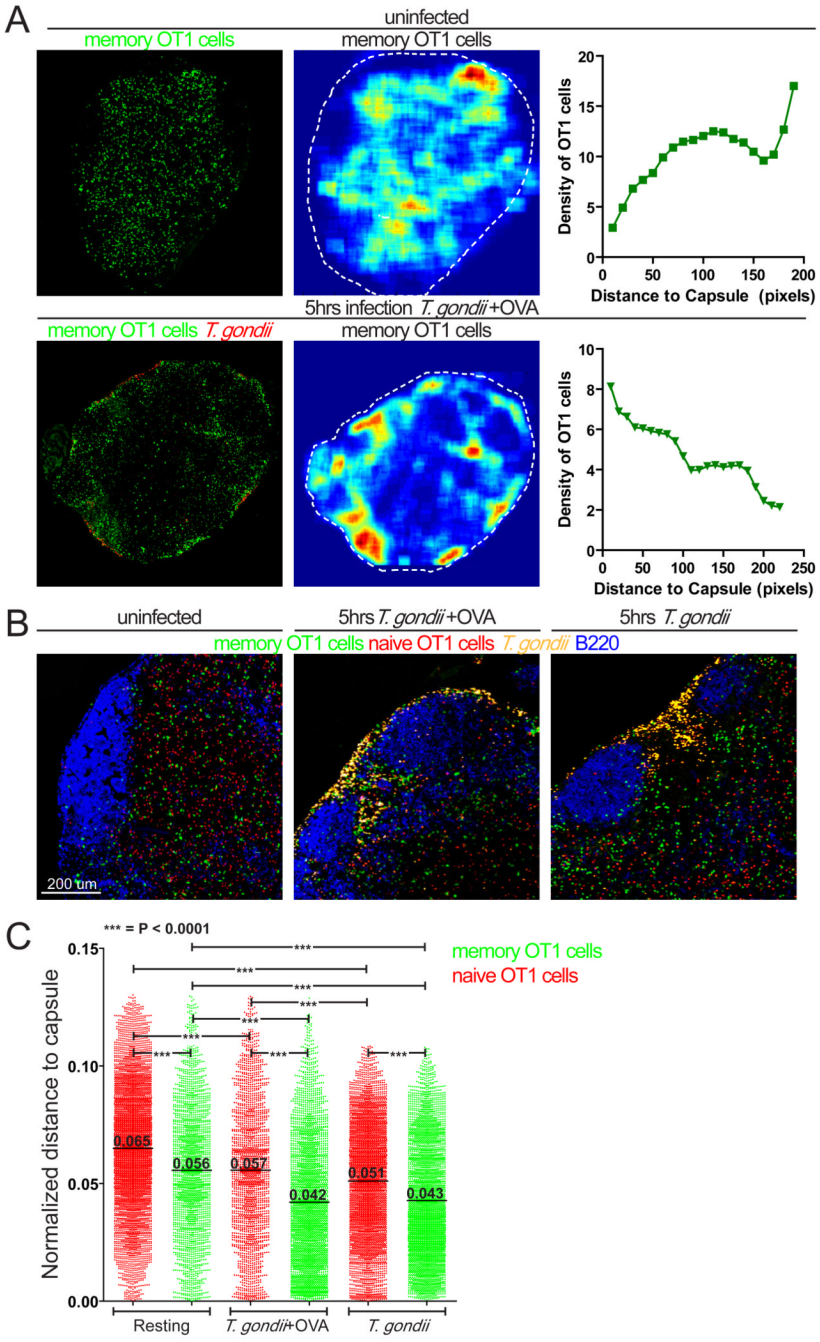

Figure 1. Memory T cells localize to sites of infection near the lymph node capsule

Confocal analysis of lymph nodes from immunized mice containing GFP-labeled OT1 memory T cells (green) either resting or 5 hours after ear-flap challenge with *T. gondii.* A) Confocal images of resting lymph nodes (top panel) and lymph nodes after ear-flap challenge with *T. gondii*+OVA (red) (bottom panel). Middle panels show memory T cell distribution as density maps with dotted white lines to indicate the lymph node circumference. Right panels show T cell density as a function of distance to lymph node capsule. B) Higher magnification confocal images showing naïve (red) and memory (green) T cell distribution in resting lymph nodes (left panel), and lymph nodes 5 hours after challenge with *T. gondii*+OVA (yellow, middle panel), or after challenge with *T. gondii*

without OVA (yellow, right panel). B cell areas were visualized with B220 staining (blue). C) Naïve and memory T cell distribution in sections shown in (B). The distance from a T cell to lymph node capsule was divided by the lymph node circumference and expressed as normalized distance. Each point on the graph represents an individual T cell and are compiled from 1–2 lymph nodes each. Data for individual quadrants of lymph nodes are provided in Fig. S3

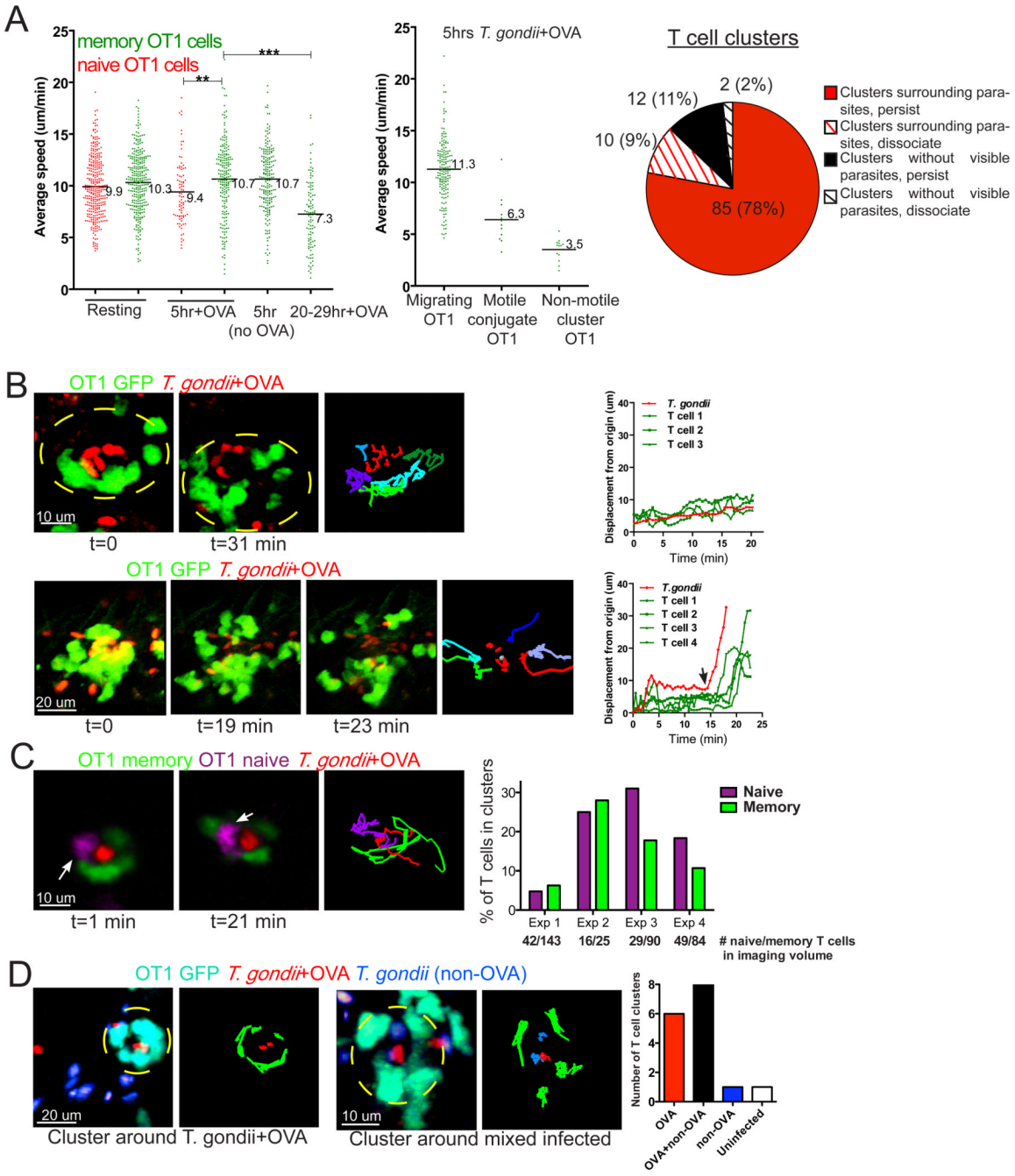

Figure 2. Memory T cells form stable conjugates with *T. gondii*- infected cells

A) Naïve and memory T cell migration before and after challenge with *T. gondii.* Draining lymph nodes from mice containing GFP-labeled OT1 memory T cells and SNARF-labeled OT1 naïve T cells were imaged using 2-photon microscopy either in resting state or at indicated times after challenge. The graph on the left shows the average speed of naïve (red) and memory (green) T cells under the indicated conditions (***p<0.0001, **p=0.0064). Middle graph shows average speed of memory T cells from a lymph node 5 hours after challenge with *T. gondii*+OVA with T cells categorized based on types of contacts formed. The pie graph summarizes the types of T cell clusters observed in 42 datasets. B–C) Mice containing GFP-labeled OT1 memory T cells (green) were challenged with *T. gondii*+OVA

parasites (red) 5 hours prior to analysis. In some experiments mice were transferred with naive OT1 CFP lymphocytes 24 hours before challenge. B) Examples of T cell clusters from a lymph node 5 hours after challenge. Top panel shows an example of a memory T cell cluster around a cell infected with parasites that persists for the length of the imaging run (31 min). Bottom panel shows a T cell cluster that disperses during the imaging run. Right hand images show the paths for parasites (red) and T cells (various colors). The graphs on the right show displacement from origin for parasite and T cells. Black arrow indicates the time point at which cluster dispersal was first observed.
Corresponds to video 2B–C. C) A cluster containing both memory (green) and naïve T cells (magenta, white arrow). 2-D projections of 3-D two-photon imaging volumes are shown at time frames indicated, and colored lines represent tracks of individual T cells or parasite. Plot shows the number of naive or memory T cells in clusters as a percentage of the total number of naive or memory T cells in the imaging volume for 4 different imaging runs. Numbers under bars indicate the total number of naïve or memory T cells present in each imaging volume. Corresponds to video 2B–C. D) Mice containing GFP-labeled OT1 memory T cells (cyan) were challenged via earflap with one-to-one mixtures of *T. gondii* +OVA expressing RFP (red) and control -OVA parasites expressing YFP (blue) and lymph nodes were imaged 5 hours later. Left panel show representative memory T cell clusters surrounding OVA only (left panels) or surrounding mixed + and − OVA parasites infected cells (right panels).
Corresponds to video 2D. Graph shows the total number of T cell clusters scored in each category for 12 separate runs.

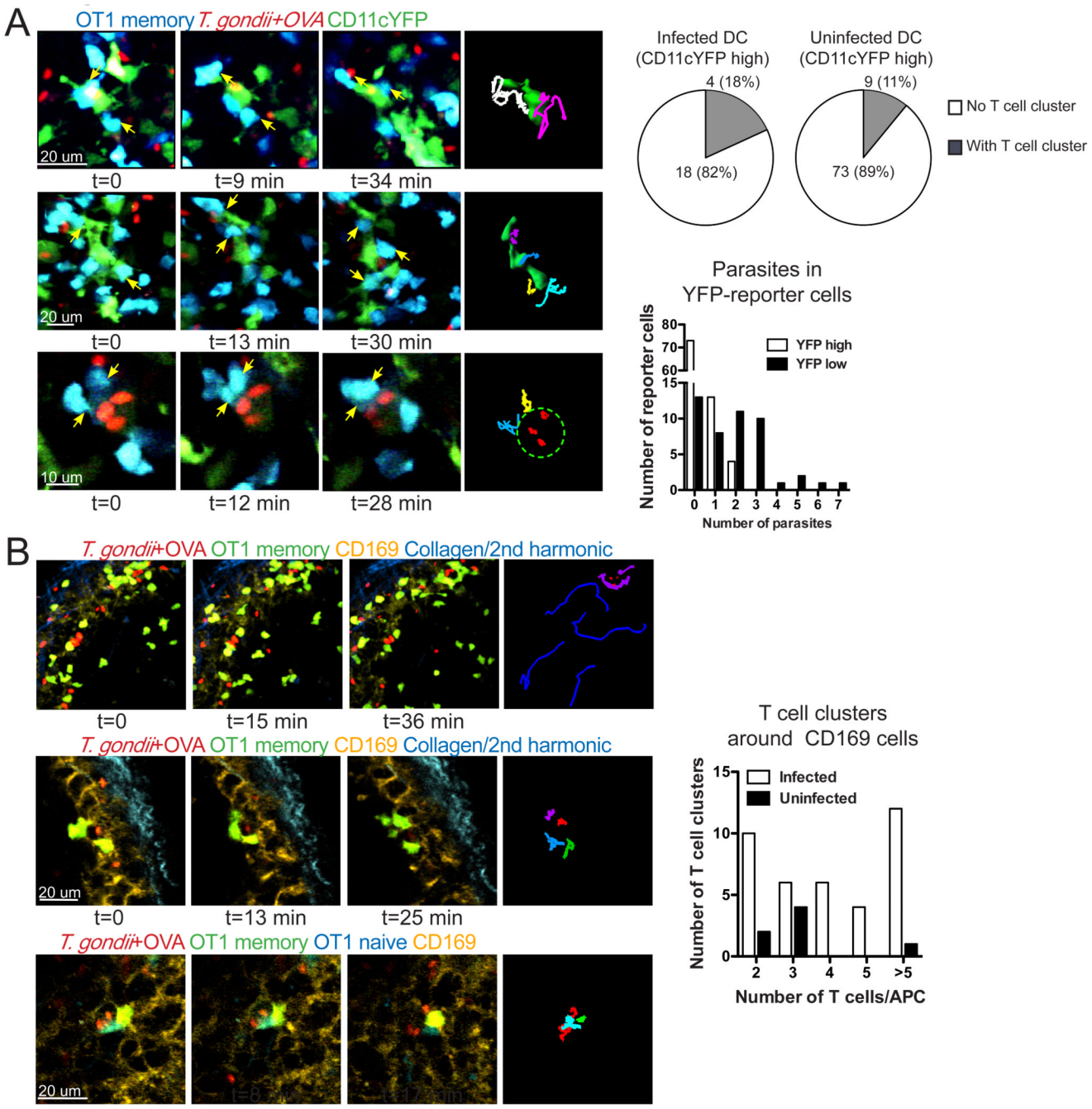

Figure 3. T cells form long-lasting interactions with SCS macrophages and DCs after challenge

A) OT1 memory T cells form long-lasting interactions with CD11c YFP high infected (top panel) and uninfected (middle panel) DCs, and YFP low cells (bottom panel). Arrows show memory OT1 T cells (blue) engaged in long-lasting contacts with APCs (green). 2-D projections of 3-D two-photon imaging volumes are shown at time frames indicated. Corresponds to video 3A. Right hand images show the paths for T cells (various colors) in contact with YFP high (shown in green, top and middle panels) or YFP low (indicated by red tracks, circled in green, bottom panel) cells. Pie charts summarize the number of infected (left) and uninfected (right) CD11cYFPhigh DCs that supported T cell clusters in 11 datasets. The graph shows the numbers of parasites in YFP high and low cells. CD11c YFP

reporter mice containing GFP-labeled OT1 memory T cells were challenged with *T. gondii* +OVA 5 hours before explanting the draining lymph node for imaging. B) OT1 T cells form clusters around infected CD169 cells. Mice containing GFP-labeled OT1 memory T cells were challenged with *T.gondii*+OVA (red) for 5 hours and injected with CD169-Alexa 532 5 min prior to explanting of draining lymph nodes for imaging. In some experiments mice were also transferred with CFP-labeled OT1 naive T cells 24 hours prior to challenge. Two-photon images of OT1 memory T cells (green) in stable interactions with CD169 (yellow), with second harmonic signal from the collagen-rich capsule shown in blue. Right hand images show the tracks for *T. gondii* (red) and OT1 T cells (various colors). Z-projections of an imaging volume are shown at indicated times.
Corresponds to video 3Bi. Middle panels show higher magnification images of OT1 memory T cells interacting with an infected CD169 cell. Single optical sections of an imaging volume are shown at indicated times. The graph shows the distribution of T cell cluster sizes around CD169 cells. Bottom panels show a cluster consisting of a naïve (blue) and a memory (green) OT1 T cells forming a cluster around an infected CD169 cell (yellow). Corresponds to video 3Bii.

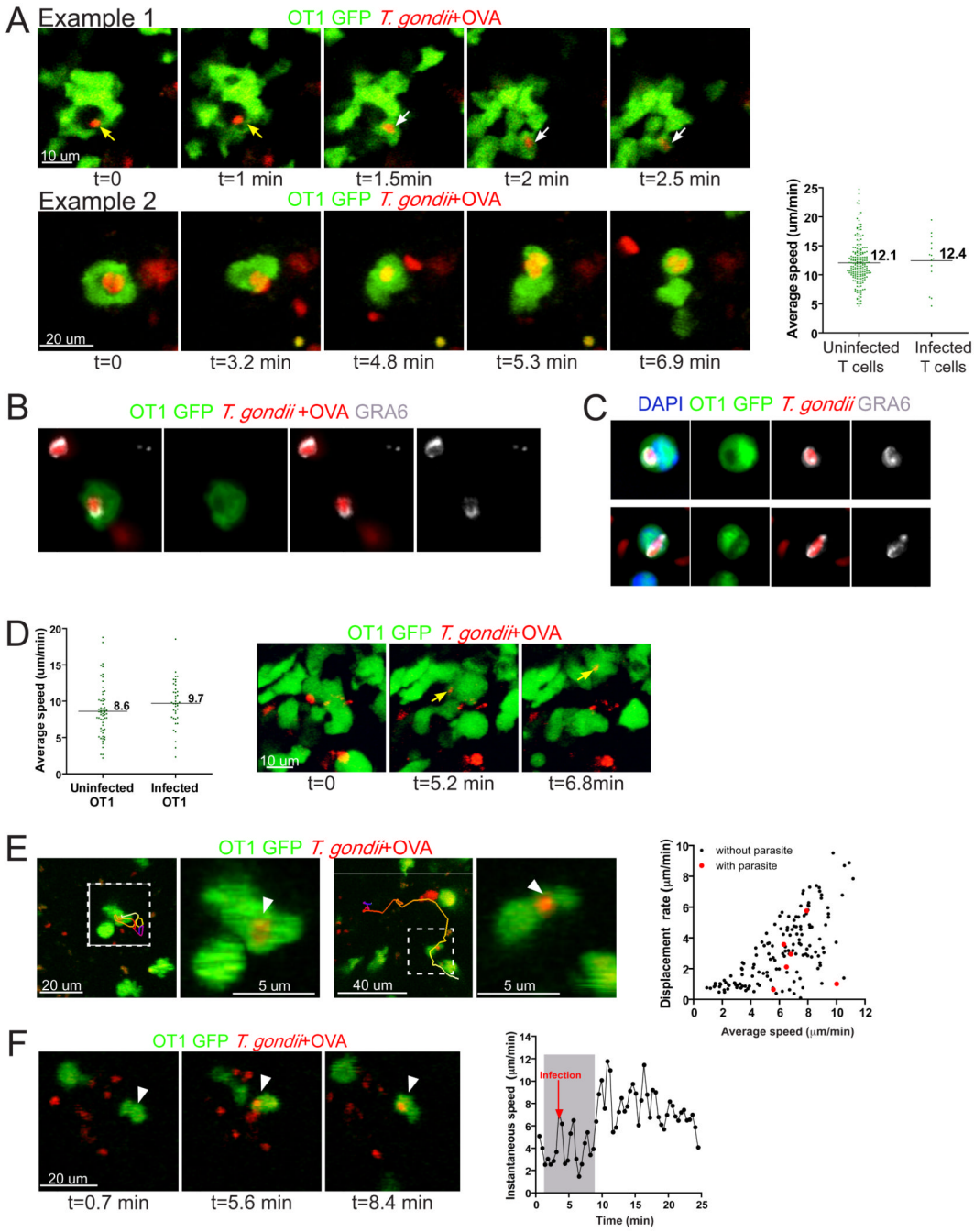

Figure 4. Direct invasion of T cells during contacts with infected host cells

A) Two examples of T cell invasion during interactions with infected APCs in draining lymph nodes following earflap infection. Single optical sections from two-photon imaging runs showing memory OT1 GFP T cells (green) being invaded by parasites (red). In the top panel, yellow arrows point to the parasite prior T cell invasion while white arrows indicate the parasite inside the T cells. Corresponds to video 4A. Right hand panel shows average speeds of individual T cells containing parasite fluorescence signal (infected T cells) compared to T cells without parasite signal (uninfected T cells) from the same imaging volumes. B, C) Immunofluorescence images of infected T cells stained for the parasite dense granule protein, GRA6 as a marker for the parasitophorous vacuole. RFP-labeled parasites

are shown in red, GFP labeled T cells are in green, and GRA6 immunostaining is shown in white. B) Confocal analysis of the lymph node samples described in (A). C) In vitro infected T cells with nuclei labeled with DAPI (blue). D) Naïve mice containing GFP-labeled OT1 T cells were orally infected with *T. gondii*+OVA cysts for 5–7 days prior to explanting of mesenteric lymph nodes for imaging. Average speed of infected and uninfected OT1 T cells in the mesenteric lymph nodes determined by analysis of two-photon imaging data. Right panels show OT1 T cell (green) invasion by *T. gondii*+OVA (red) in the mesenteric lymph nodes 5 days after oral infection with 75 cysts. Single optical sections of two-photon imaging volumes are shown. E) Dynamic imaging of OT1 T cells containing parasites in vibratome-cut brain slices from chronically infected mice. Left panels show projections of imaging volumes from time-lapse series obtained by two-photon microscopy. Dashed boxes indicate invaded T cells, with enlarged views to show the parasite fluorescence (arrowhead). The paths of infected OT1 GFP cells are depicted by color-coded lines to depict time (blue-red-yellow-white). Right most panel shows a plot of displacement rate, versus the average speed for individual T cells. Red circles are infected OT1 T cells and black circles are OT1 T cells without visible parasite fluorescence from the same runs. Data was generated 4 different samples, 10 to 39 days p.i. F) An example of an OT1 cell being invaded by a parasite in the brain. Three frames from a time-lapse sequence are shown before (left panel), during (center panel), and after (right panel) invasion. The arrow indicates the position of the OT1 GFP T cell at each time point. Plot on right shows the instantaneous speed versus time of the T cell. Shaded area corresponds to the time the T cell stops near the group of isolated parasites. Red arrow indicates the time point at which the parasite is first seen inside the T cell. Corresponds to Video 4D–F.

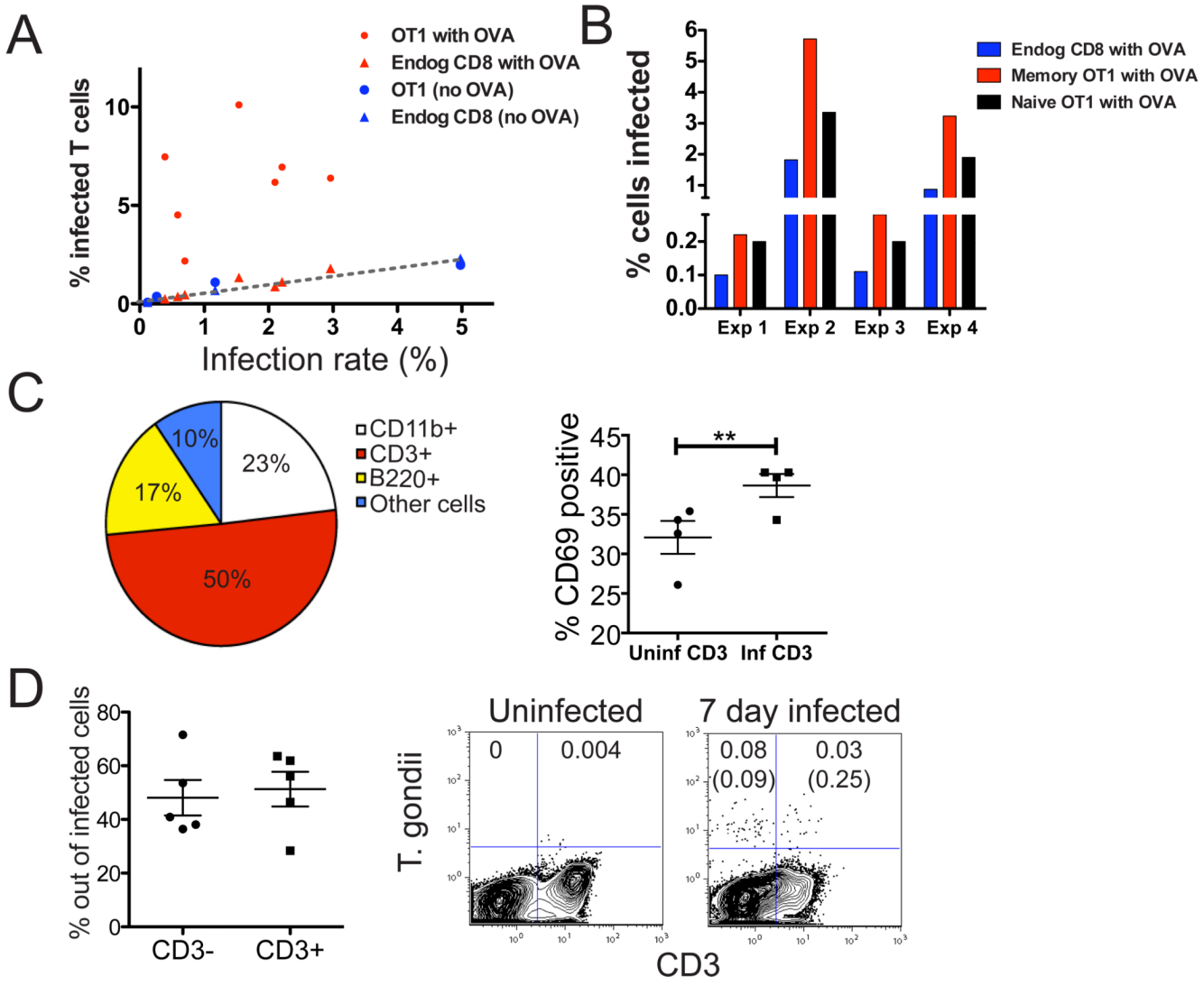

Figure 5. Antigen recognition enhances T cell invasion by *T. gondii*

A) Flow cytometric analyses showing the % of infected cells as a proportion of gated OT1 T cells (circles) or endogenous, polyclonal T cells (triangles) in draining lymph nodes of mice challenged via earflap with OVA-expressing parasites (red) or parasites without OVA (blue) 24 hours before analysis. Graph shows the % of gated T cells containing parasite fluorescence (% infected T cells) plotted as a function of infection rate. Each point represents the indicated T cell population from a single lymph node.. B) Flow cytometric analysis comparing the infection rates of naive and memory OT1 T cells for 4 individual lymph nodes. Mice were challenged with OVA expressing parasites 24 hours before analysis. C, D) Naïve mice were infected orally with 50- 75 *T. gondii* cysts and analyzed 5–7 days later. C) Flow cytometric analysis of mesenteric lymph nodes. Pie chart shows the proportions of parasites contained in different leukocyte subsets in the mesenteric lymph nodes, and plot on right shows CD69 expression in uninfected or infected CD3+ cells. **p=0.0027 D) Flow cytometric analysis of CD3 and parasite fluorescence in blood leukocytes. Left panels show compiled data and right panels show representative FACS plots. Uninfected mice are shown for comparison. The numbers indicate % of infected cells

out of total live gate, the numbers in brackets are % of infected cells out of CD3- and CD3+ populations respectively.

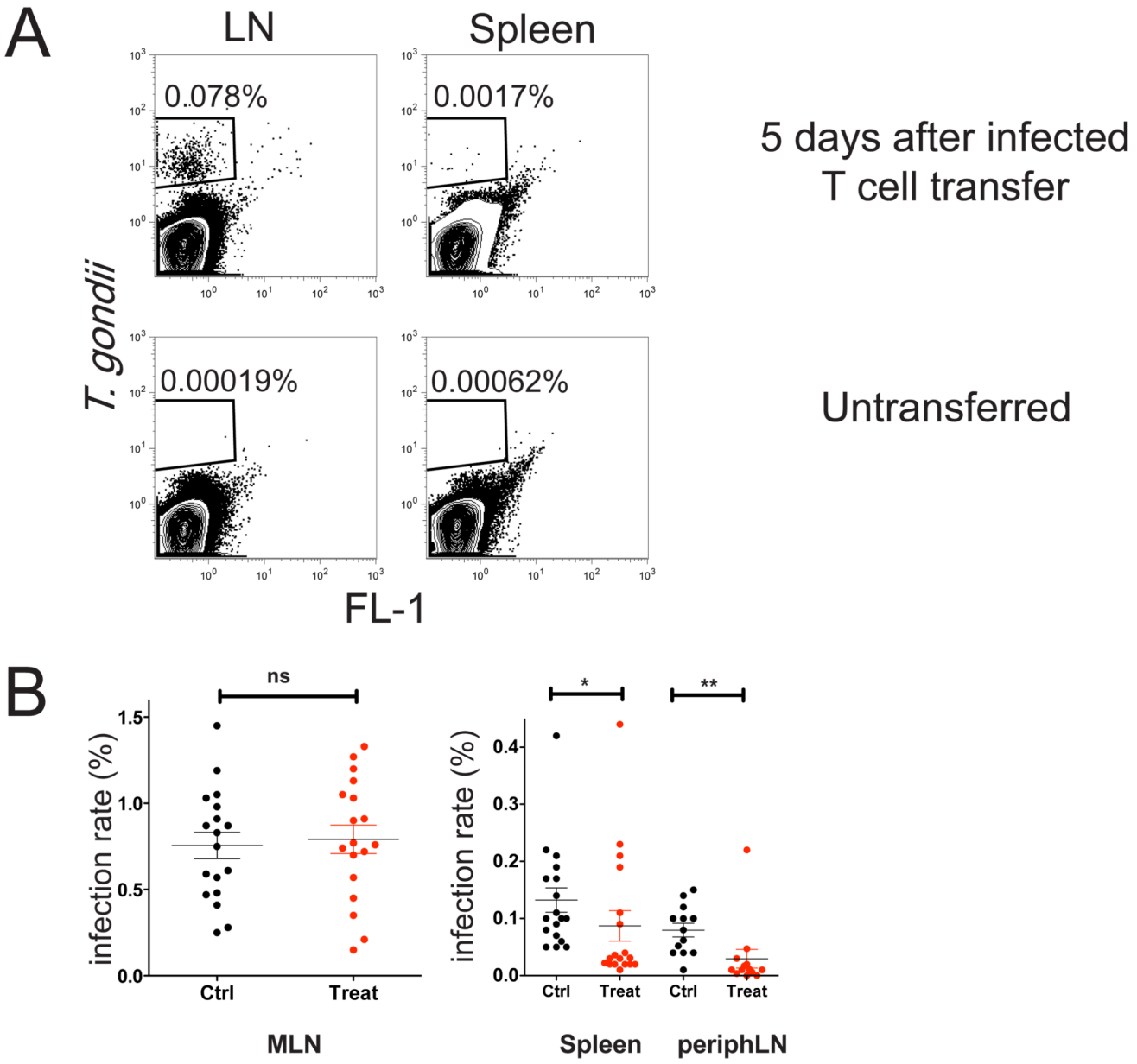

Figure 6. Evidence for parasite spread via invaded T cells

A) Parasite-containing CD8 T cells were isolated from the mesenteric lymph nodes of mice that had been infected orally (7 days earlier) and 10,000 FACS-sorted infected T cells were injected via the earflap of a naive mouse. Five days later mice draining lymph nodes and spleens were analyzed by flow cytometry. Mice that did not receive infected T cells are shown for comparison.

B) Mice were orally infected with 50–75 cysts from RFP parasites (day 0) and treated on days 1, 3, 5 with FTY720, and on day 7, infection rates were determined by by flow cytometry of collagenase-dissociated spleen and lymph nodes. *p=0.0018, **p=0.0001. Peripheral blood of treated mice showed a 4 fold decrease in the number of T cells in treated compared to control mice, (data not shown) indicating an efficient and selective block in T cell egress from lymph nodes.